bioRxiv preprint doi: https://doi.org/10.1101/780791; this version posted September 24, 2019. The copyright holder for this preprint (which was not certified by peer review) is the author/funder, who has granted bioRxiv a license to display the preprint in perpetuity. It is made available under aCC-BY-NC-ND 4.0 International license.

Chikungunya virus infection impairs osteogenic differentiation of bone marrow-derived mesenchymal stem cells

Enakshi Roy[1], Wen Shi[2], Bin Duan[2*], St Patrick Reid[1*]

[1]Department of Pathology & Microbiology, University of Nebraska Medical Center, Omaha, NE 68198-5900, USA

[2]Mary & Dick Holland Regenerative Medicine Program, Division of Cardiology, Department of Internal Medicine, University of Nebraska Medical Center, Omaha, NE 68198-5900, USA

*Corresponding authors- St Patrick Reid, patrick.reid@unmc.edu; Bin Duan, bin.duan@unmc.edu

bioRxiv preprint doi: https://doi.org/10.1101/780791; this version posted September 24, 2019. The copyright holder for this preprint (which was not certified by peer review) is the author/funder, who has granted bioRxiv a license to display the preprint in perpetuity. It is made available under aCC-BY-NC-ND 4.0 International license.

Abstract

Chikungunya virus (CHIKV) is a positive-sense, single-stranded RNA virus, belonging to the genus alphavirus in the family *Togaviridae*. The virus is spread by the *Aedes* species (sp.) mosquitoes in tropical and subtropical regions of the world. CHIKV causes Chikungunya fever (CHIKF), where the acute stage of infection is characterized by high fever, headache, rash, and polyarthralgia. In 30-40% of cases, patients develop a chronic stage with debilitating joint pain persisting for months to years imposing a burden on the population in terms of disability adjusted life years (DALY). Presently, no vaccines or treatment options are available for this infection. Prior investigations reveal that CHIKV infection is associated with bone pathology; however, the molecular mechanism underlying CHIKV-induced bone pathology remains poorly defined. Studies show that disruption of osteogenic differentiation and function of bone marrow-derived mesenchymal stem cells (BMMSCs) can lead to bone pathologies. However, to date pathogenesis of CHIKV infection in this context has not been studied. In the current study, we investigated the susceptibility of BMMSCs to CHIKV and studied the effect of infection on BMMSCs-derived osteogenic cells. To our knowledge, for the first time we report that CHIKV can productively infect BMMSCs. We observed a decrease in the intracellular and extracellular alkaline phosphatase (ALP) activity and reduction in calcium phosphate deposition in infected cells compared to mock-infected control. Thus, we conclude that CHIKV infects BMMSCs and disrupts function of osteogenic cells.

bioRxiv preprint doi: https://doi.org/10.1101/780791; this version posted September 24, 2019. The copyright holder for this preprint (which was not certified by peer review) is the author/funder, who has granted bioRxiv a license to display the preprint in perpetuity. It is made available under aCC-BY-NC-ND 4.0 International license.

Importance

Although studies have shown association of bone pathology and CHIKV infection, the pathogenesis of infection causing altered bone homeostasis is not fully understood. Here, we demonstrate for the first time that BMMSCs are susceptible to CHIKV infection. Furthermore, we observe that infection causes disruption in the function of BMMSC- derived osteogenic cells. Impaired function of these osteogenic cells will likely lead to a disruption in bone homeostasis and in part, provides a mechanism for the observed bone pathology associated with CHIKV pathogenesis.

Keywords

Chikungunya virus, mesenchymal stem cells, osteogenic differentiation

bioRxiv preprint doi: https://doi.org/10.1101/780791; this version posted September 24, 2019. The copyright holder for this preprint (which was not certified by peer review) is the author/funder, who has granted bioRxiv a license to display the preprint in perpetuity. It is made available under aCC-BY-NC-ND 4.0 International license.

Introduction

Chikungunya virus (CHIKV) is a positive-sense, single-stranded RNA virus belonging to the *Togaviridae* family and alphavirus genus (1) (2). Since the mid-1900s, there have been outbreaks of CHIKV infection in Africa, Asia, and the Indian and Pacific Ocean region, with few reported cases within Europe (3). Beginning in 2013, there have been increasing numbers of infections in the Americas, in part due to travel from affected region (4). CHIKV is transmitted by *Aedes* species (sp). Mosquitoes. CHIKV infection in the tropical and subtropical regions of the world can lead to Chikungunya fever (CHIKF) (5). CHIKF is characterized by a self-limiting acute stage, with symptoms of fever, rash and arthralgia which lasts for 1-2 weeks (6). In 30-40% of cases, infected individuals develop an incapacitating chronic arthritic stage which may persist for months to years, thereby imposing a burden on the population in terms of disability adjusted life years (DALY) (7-10)

Recent studies identified bone lesions in the joints of CHIKV infected mice, indicating that CHIKV can cause bone pathologies (11, 12). In another study, mice infected with a similar arthritogenic alphavirus, Ross River virus (RRV) resulted in significant bone loss. (13). In humans, magnetic resonance imaging (MRI) studies revealed that CHIKV infection is associated with erosive arthritis (14, 15). Taken together, these studies suggest alphavirus infection can affect bone homeostasis and thus contribute to arthritic-like conditions.

Mesenchymal stem cells (MSCs) are multipotent, non-hematopoietic stromal cells which can self-renew and differentiate into various cell lineages (16). MSCs can be derived from umbilical cord blood, adipose tissue and bone marrow (16). Bone marrow-

bioRxiv preprint doi: https://doi.org/10.1101/780791; this version posted September 24, 2019. The copyright holder for this preprint (which was not certified by peer review) is the author/funder, who has granted bioRxiv a license to display the preprint in perpetuity. It is made available under aCC-BY-NC-ND 4.0 International license.

derived MSCs (BMMSCs) have trilineage differentiation potential and they can differentiate into osteogenic, chondrogenic or adipogenic cell lineage (17). The osteogenic differentiation of BMMSCs is important for bone-remodeling, and the inability of BMMSCs to differentiate into the osteogenic lineage may lead to an imbalance in bone remodeling and eventually bone loss (18-20). A few studies have shown that virus infection of BMMSCs can affect the properties and function of these cells (21, 22).

In this study, we investigated the susceptibility and response of BMMSCs to CHIKV infection. We hypothesized that CHIKV can infect BMMSCs and affect the osteogenic differentiation of BMMSCs. Our results show that CHIKV can productively infect BMMSCs. Importantly, we observed that viral infection significantly impaired the function of the osteogenic cells, as evidenced by the decrease in alkaline phosphatase (ALP) activity at 14 days post infection (dpi) and rate of mineralization at 7 and 14 dpi compared to mock-infected control. Together, these findings indicate CHIKV can infect BMMSCs and disrupt BMMSC-derived osteogenic cell function.

Results

BMMSCs are permissive to CHIKV infection

CHIKV infection has been associated with bone pathology, implying its role in disruption of bone homeostasis (11, 12, 14, 15). BMMSC-derived osteogenic differentiation is essential for bone homeostasis (18-20). Recent studies show that viral infection can affect the function of BMMSCs and BMMSC-derived osteogenic cells (21, 22). However, to date, it is unknown whether alphaviruses can infect BMMSCs and disrupt osteogenic cell function. Permissivity of BMMSCs to CHIKV infection was

bioRxiv preprint doi: https://doi.org/10.1101/780791; this version posted September 24, 2019. The copyright holder for this preprint (which was not certified by peer review) is the author/funder, who has granted bioRxiv a license to display the preprint in perpetuity. It is made available under aCC-BY-NC-ND 4.0 International license.

110 determined by infecting cells under acute infection condition (Fig.1). To detect the
111 presence of infection in BMMSCs, immunofluorescence assays (IFA) were performed
112 at 24 hours post-infection (hpi). Infection was confirmed by visualizing the presence of
113 viral non-structural protein 4 (nsP4) in infected cells at all MOIs tested (Fig. 2A). To
114 detect replication of virus in infected cells, the expression of viral non-structural protein 1
115 (nsP1) gene was quantified by qRT-PCR. Infected cells showed a significant increase in
116 nsP1 gene expression at 24 hpi with increased MOIs (Fig. 2B). Morphological analysis
117 of infected cultures at 48 hpi showed the presence of cytopathic effect (CPE),
118 particularly at higher MOIs (Fig. S1A). CPE was quantified at 48 hpi using
119 Viral ToxGlo assay by determining ATP content. Higher MOIs (0.1 and 1.0) resulted in
120 significant CPE as evidenced by the decrease in luminescence signal (Fig. S1B). Lower
121 MOIs (0.001 and 0.01) resulted in productive viral infection as evidenced by IFA and
122 qRT-PCR with minimal CPE. Collectively, these data indicate that BMMSCs are
123 susceptible to CHIKV infection.
124
125 **CHIKV infection interferes with function of osteogenic cells**
126 **BMMSC-derived osteogenic cells are susceptible to CHIKV infection**
127 Osteogenic differentiation of BMMSCs plays an important role in bone
128 homeostasis (18-20). In addition, viral infection have been associated with altered
129 function of BMMSC-derived osteogenic cells (21). Therefore, we next investigated the
130 fate of CHIKV-infected, differentiated BMMSCs. Based on our initial data we selected a
131 MOI of 0.001 and 0.01 for further “chronic infection” experiments. Cells were infected
132 and differentiated as described in Figure 1. Osteogenic differentiation was confirmed by

bioRxiv preprint doi: https://doi.org/10.1101/780791; this version posted September 24, 2019. The copyright holder for this preprint (which was not certified by peer review) is the author/funder, who has granted bioRxiv a license to display the preprint in perpetuity. It is made available under aCC-BY-NC-ND 4.0 International license.

Alizarin Red staining assay. This assay detects the deposition of calcium phosphate crystals, formed during matrix mineralization by osteogenic cells (23). Presence of red stained calcium nodes was clearly detected in differentiated cells at 7 and 14 days post differentiation (dpd) compared to undifferentiated controls (Fig 3). To determine the susceptibility of the osteogenic cells to CHIKV infection, viral replication was confirmed by nsP1 gene expression using qRT-PCR at 7 dpi. A significant increase in nsP1 expression was observed in infected cells compared to mock (Fig. 3B). Next, we confirmed the production of infectious virus particles at 7 dpi by plaque assay (Fig. 3C). Similarly, we observed an increase in infectious virus particle production. We next determined the viability of the osteogenic cells during infection. Brightfield images of infected cells at 7 dpi showed evidence of CPE, particularly at MOI 0.01 (Fig. 3D). Interestingly, CPE quantification done by Viral ToxGlo assay resulted in minimal CPE production when compared to mock-infected cells at 7 dpi (Fig. S2A). Morphological analysis and CPE quantification at 14 dpi showed similar results (Fig. S2B and C). Taken together, these results demonstrate that osteogenic cells are susceptible to CHIKV infection and results in minimal CPE at low MOIs.

CHIKV infection impairs function of osteogenic cells

Prior studies have shown viral infection of osteogenic cells causes impaired ALP activity during differentiation (21). To examine the effect of CHIKV infection on ALP activity, BMMSCs were infected as previously outlined (Fig 1). ALP activity and ALP staining assays were performed. No significant change in ALP activity was observed in infected cells at 7 dpi (Fig. 4A). However, a significant reduction in the ALP activity was observed in infected cells at 14 dpi (Fig. 4B). The infected cells resulted in reduced ALP

bioRxiv preprint doi: https://doi.org/10.1101/780791; this version posted September 24, 2019. The copyright holder for this preprint (which was not certified by peer review) is the author/funder, who has granted bioRxiv a license to display the preprint in perpetuity. It is made available under aCC-BY-NC-ND 4.0 International license.

156 staining intensity at both 7 and 14 dpi (Fig. 4C). Next we performed Alizarin Red
157 staining assay to detect the effect of viral infection on deposition of calcium phosphate
158 crystals. BMMSC were infected as described in Figure. 1 and Alizarin Red staining
159 assay was done at 7 and 14 dpi. A significant decrease in calcium phosphate deposits
160 was observed in infected cells at 7 and 14 dpi (Fig. 4D). Together, these results
161 demonstrate for the first time that CHIKV infection impairs the function of BMMSC-
162 derived osteogenic cells.

163 **Discussion**

164 Joint pathology and arthritic-like conditions are associated with CHIKV infection,
165 however the mechanism underlying these conditions remains poorly defined (11, 12, 14,
166 15, 24). BMMSCs are non-hematopoietic multipotent stem cells which can differentiate
167 into adipogenic, osteogenic, and chondrogenic lineages (16, 17). These cells can
168 secrete and respond to different signaling molecules and undergo osteogenic
169 differentiation thereby playing an essential role in bone homeostasis (18, 25). Previous
170 studies have shown that virus infection can affect functions of BMMSCs (21, 22, 26), but
171 it is unclear whether BMMSCs are susceptible to alphavirus infection.

172 Osteogenic cells will terminally differentiate into osteoblasts (18, 23). A prior
173 report demonstrated that osteoblasts are susceptible to CHIKV infection (27). However,
174 it is unclear whether osteoblast progenitor cells are susceptible to infection. Moreover,
175 whether infection affects differentiation and/or function. The results of our study
176 demonstrate that both BMMSCs and BMMSC-derived osteogenic cells are susceptible
177 to CHIKV infection. Prior studies have shown that viral infection of BMMSCs can alter
178 function, therefore we hypothesize that ability of CHIKV to infect these cells will similarly

bioRxiv preprint doi: https://doi.org/10.1101/780791; this version posted September 24, 2019. The copyright holder for this preprint (which was not certified by peer review) is the author/funder, who has granted bioRxiv a license to display the preprint in perpetuity. It is made available under aCC-BY-NC-ND 4.0 International license.

affect function (22). In our preliminary experiments, we observed CPE during infection of both BMMSCs and osteogenic cells at relatively high MOI. However, minimal CPE was observed at low MOI. We therefore selected lower MOI infections for our chronic infection experiments.

Previous studies demonstrated that viral infection causes impaired matrix mineralization and ALP activity (21, 22). Our study revealed that despite a lack of significant change in ALP activity at 7 dpi, there was a significant reduction in ALP activity at 14 dpi. Moreover, reduction in ALP staining intensity was observed at both 7 and 14 dpi. The results obtained are similar to a prior study showing the effect of viral infection on ALP activity (21). The lack of significant change in ALP activity at 7 dpi was likely due the observed absence of a difference in ALP activity between undifferentiated and differentiated osteogenic cells at 7 dpd (data shown). Calcium phosphate deposition due to mineralization is a hallmark of osteogenic differentiation (23, 28). We found that at 7 and 14 dpi, CHIKV caused a significant reduction in calcium phosphate deposition in infected cells. This indicates that CHIKV infection disrupts the mineralization function of osteogenic cells, in that way likely disrupts bone homeostasis. It is important to note that matrix mineralization is also associated with the production of extracellular matrix (ECM) proteins including fibronectin, vitronectin, laminin, osteopontin, and osteonectin (23, 28-30). Thus, future studies will be aimed at examining the expression and production of these proteins in the context of viral infection.

In vivo differentiation of BMMSCs into the osteogenic cell lineage depends on their interaction with other cells in the joint space (23, 31-33). Hence, co-culturing of

bioRxiv preprint doi: https://doi.org/10.1101/780791; this version posted September 24, 2019. The copyright holder for this preprint (which was not certified by peer review) is the author/funder, who has granted bioRxiv a license to display the preprint in perpetuity. It is made available under aCC-BY-NC-ND 4.0 International license.

202 BMMSCs with cells, including osteoclasts, synovial fibroblasts, macrophages and
203 chondrocytes in the presence of CHIKV will lead to a better understanding the
204 mechanism underlying the disruption of bone homeostasis (34-36).

205 It is well established that the receptor activator of nuclear factor kappa-B ligand
206 (RANKL)/osteoprotegerin (OPG) ratio plays an important role in bone homeostasis and
207 drives osteoclastogenesis (37-40), the dysregulation of which likely contributes to
208 CHIKV-induced bone pathology. It has been reported that CHIKV infection of
209 osteoblasts can alter RANKL/OPG ratio (41). Based on our findings, it will be interesting
210 to examine the contribution of CHIKV infection of osteoblast progenitors *in vitro* and *in*
211 *vivo* and the effect on RANKL/OPG levels.

212 In our study, we report that BMMSCs are susceptible to CHIKV infection, and
213 infection impairs ALP activity and calcium phosphate deposition in osteogenic cells. Our
214 results indicate that CHIKV infection leads to functionally altered osteogenic cells and
215 likely leads to dysregulation in bone homeostasis. Thus, studying BMMSCs in the
216 context of CHIKV infection can serve as an appropriate model for better understanding
217 viral-induced bone pathology.

218

219 **Materials and Methods**

220 **Cell culture, Compounds and Virus**

221 Human BMMSCs were purchased from Roosterbio (USA). CHIKV (181/25 clone)
222 was purchased from BEI Resources (USA).

223 BMMSCs were infected at MOI 0.001, 0.01, 0.1 or 1 and incubated for 1 h at
224 37°C, 5% CO_2. At one-hour post infection (hpi), cells were washed with DPBS (Corning,

bioRxiv preprint doi: https://doi.org/10.1101/780791; this version posted September 24, 2019. The copyright holder for this preprint (which was not certified by peer review) is the author/funder, who has granted bioRxiv a license to display the preprint in perpetuity. It is made available under aCC-BY-NC-ND 4.0 International license.

USA), replenished with Rooster Basal MSC (RBM) media (RoosterBio, USA) and incubated at 37°C, 5% CO_2 for 2 days for proliferation. For the purposes of this study, the 2-day incubation period was considered an acute infection (Fig. 1).

For differentiation study, BMMSCs were infected at MOI 0.001 or 0.01 and incubated for 1 h at 37°C, 5% CO_2. After 1 hpi, cells were washed with DPBS, replenished with osteogenic differentiation media containing mesenchymal stem cell expansion medium (Millipore, USA) and supplemented with 10 mM beta glycerophosphate (Sigma, USA), 0.1 µM dexamethasone (Sigma, USA) and 200 µM ascorbic acid (Sigma, USA). Media change was done every 2 dpi. For this study, this was considered as a chronic infection (Fig. 1). For these experiments, mock-infected undifferentiated cells were negative controls, while mock-infected differentiated cells were positive controls.

Baby hamster kidney cells (BHK-21; ATCC CCL10) were cultured in Dulbecco's modified Eagle's medium (DMEM) (Invitrogen, USA) and supplemented with 10% Fetal bovine serum (FBS) (Gibco, USA)

Determination of CPE

Cells at a density of 1×10^5 per well were seeded in 6-well plates and incubated for 24 h, at 37°C. A confluent monolayer of cells were infected under both acute and chronic conditions as mentioned above. To determine CPE, infected cells were observed using the DM1/MC120 bright field microscope (Leica, Germany). Images were collected every 24 h for acute infection and at 7 and 14 dpi for chronic infection.

The viral CPE was quantified by the Viral ToxGlo assay (Promega, USA). This assay detects the amount of ATP produced by the cells (42). CPE produced due to viral

bioRxiv preprint doi: https://doi.org/10.1101/780791; this version posted September 24, 2019. The copyright holder for this preprint (which was not certified by peer review) is the author/funder, who has granted bioRxiv a license to display the preprint in perpetuity. It is made available under aCC-BY-NC-ND 4.0 International license.

248 infection leads to decreased ATP production which can be quantified. Cells at a density
249 of 3×10^3 per well were seeded in a 96-well plate and incubated for 24 h at 37°C. For
250 quantification of CPE in acute infection, Viral Tox Glo assay was performed at 48 hpi,
251 and for chronic infection, the assay was performed at 7 and 14 dpi, according to
252 manufacturer's instructions. The change in ATP production in infected versus mock-
253 infected BMMSCs was measured using a Tecan Spark® microplate luminometer
254 (Tecan Trading AG, Switzerland).

255 **Immunofluorescence assay**

256 Cells at a density of 2.5×10^4 per well were seeded in 4-well plate containing
257 glass cover slips in each well and incubated for 24 h, at 37 °C. Mock or virus-infected
258 cells were fixed in 4% paraformaldehyde (PFA) (Electron Microscopy Sciences, USA)
259 for 30 min and permeabilized with 0.1% Triton X (Fisher Bioreagents, USA) for 10 mins.
260 Blocking was done in 3% Bovine Serum Albumin-Phosphate Buffered Saline
261 (PBS/BSA) for 1 h. Virus was stained with antibody against CHIKV non-structural
262 protein (nsP4) (kindly provided by Dr. Andres Merits). BMMSCs were stained with
263 mouse anti-Vimentin antibody (V9) (Life Technologies, USA). Following overnight
264 incubation with primary antibody at 4°C, the cells were stained with Alexa-Fluor 568
265 goat anti-rabbit IgG and Alexa Fluor 488 donkey anti-mouse IgG (Life Technologies,
266 USA) for 1 h at room temperature. Nuclear staining was done with Hoechst 33642
267 (Invitrogen, USA) for 30 min. Images were taken and processed using Zeiss LSM 800
268 with Airyscan (Germany).

269 **ALP activity and ALP staining assay**

bioRxiv preprint doi: https://doi.org/10.1101/780791; this version posted September 24, 2019. The copyright holder for this preprint (which was not certified by peer review) is the author/funder, who has granted bioRxiv a license to display the preprint in perpetuity. It is made available under aCC-BY-NC-ND 4.0 International license.

ALP enzyme activity was determined by ALP activity assay (43). Cells at a density of 2.5×10^4 per well were seeded in a 24-well plate and incubated for 24 h at 37°C. Cells were then infected as aforementioned. At 7 and 14 dpi, the infected cells were lysed by freeze-thaw method in a buffer containing Triton X-100 (0.1% v/v) (Fischer Scientific, USA), 1 mM $MgCl_2$ (Alfa Aesar, USA), 20 mM Tris (Fischer Scientific, USA). The cell lysate was used to perform ALP activity assays using the ALP activity kit (Sigma-Aldrich, USA) according to the manufacturer's instructions. The ALP activity assay uses p-nitrophenyl phosphate (pNPP) as substrate which is dephosphorylated by the ALP enzyme forming *p*-nitrophenol which was measured spectrophotometrically at 405 nm in Synergy H1 Hybrid Reader (BioTek, USA) (43). The total protein content in the infected cells was determined using a BCA protein assay kit (Thermo Scientific, USA) with bovine serum albumin as a standard. The ALP activity was expressed as micromole of p-nitrophenol formed per 30 minutes per microgram of total protein (µmol per 30 min per µg protein).

Extracellular ALP expression was examined by ALP staining assay (44). Cells at a density of 3×10^4 per well were seeded in a 24-well plate and incubated for 24 h at 37°C. At 7 and 14 dpi, ALP staining was performed using ALP leukocyte kit (Sigma-Aldrich, USA) according to manufacturer's instructions. Images were taken using a DM1/MC120 microscope (Leica, Germany) at 20× magnification.

Alizarin Red staining

Cells at a density of 5×10^4 per well were seeded in a 24-well plate and incubated for 24 h at 37°C. At 7 and 14 dpi, Alizarin Red staining assay was performed using Alizarin Red solution (EMD Millipore, Germany) according to manufacturer's

bioRxiv preprint doi: https://doi.org/10.1101/780791; this version posted September 24, 2019. The copyright holder for this preprint (which was not certified by peer review) is the author/funder, who has granted bioRxiv a license to display the preprint in perpetuity. It is made available under aCC-BY-NC-ND 4.0 International license.

293 instructions. Alizarin Red stains the calcium phosphate deposits formed by matrix
294 mineralization during osteogenic differentiation (23). All images were taken
295 using DM1/MC120 microscope (Leica, Germany) at 20× magnification.

296 **Quantitative RT-PCR (qRT-PCR)**

297 Cells at a density of 1×10^5 per well were seeded in a 6-well plate and incubated
298 for 24 h at 37°C. For acute and chronic infection, cells were collected at 24 hpi and 7
299 dpi respectively, and lysed in RLT buffer (Qiagen, Germany) for RNA isolation. RNA
300 isolation was performed using RNeasy Mini kit (Qiagen, Germany) according to the
301 manufacturer's instructions. RNA was quantified and total RNA was reverse transcribed
302 using a qScript cDNA synthesis kit (Quantabio, USA) according to the manufacturer's
303 instructions. SYBR Green Real-Time PCR was performed on a StepOnePlus Real-Time
304 PCR System (Thermo Scientific, USA) using SSO Advanced SYBR
305 Green Supermix (Bio-Rad, USA) and primer for the nsP1 gene (Applied Biosystems,
306 USA) (5'-GGGCTATTCTCTAAACCGTTGGT-3' and 5'-
307 CTCCCGGCCTATTATCCCAAT-3') according to the manufacturer's instructions with
308 the following conditions: (i) PCR initial activation step, 95°C for 3 min, 1 cycle, and (ii)
309 three-step cycling, 95°C for 15s, followed by 60°C for 1min and 95°C for 15s, 40
310 cycles. The fold change in mRNA expression relative to mock-infected samples was
311 calculated using the 2^-ΔΔCt method. Transcript levels were normalized using
312 Hypoxanthine phosphoribosyltransferase 1 (HPRT1) (Hs02800695_m1) (Thermo
313 Scientific, USA)

314 **Plaque assay**

bioRxiv preprint doi: https://doi.org/10.1101/780791; this version posted September 24, 2019. The copyright holder for this preprint (which was not certified by peer review) is the author/funder, who has granted bioRxiv a license to display the preprint in perpetuity. It is made available under aCC-BY-NC-ND 4.0 International license.

BMMSCs at a density of 1×10^5 per well were seeded in a 6-well plate and incubated for 24 h, at 37°C. The cell culture supernatants were collected from infected and mock-infected cells at 7dpi and after serial dilution, were used to perform plaque assay. BHK21 cells were seeded into 24-well plates at a density of 1×10^5 cells per well and cultured to confluence. Confluent layer of BHK21 cells were infected in triplicate with each dilution of the culture supernatant of infected BMMSCs and incubated for 1 h and 15 min at 37°C, 5% CO_2. Cells were then overlaid with DMEM containing 5% FBS and 0.6% agarose (Fischer scientific, USA) and incubated at 37°C for 48 h. After 48 h, the agarose plugs were removed, and the cells were fixed and stained with 0.1% crystal violet solution containing 3.2% PFA. The plaques were counted, and the viral titers were expressed as plaque forming units/mL (PFU/mL).

Statistical analysis

All statistical analyses were performed using GraphPad Prism 8. Data were represented as the mean ± standard error of the mean (SEM). Significant differences between the experimental groups were determined using Student's t test. P values < 0.001 were considered significant.

Acknowledgments

We thank Dr. Leah Cook for critical reading of the manuscript and valuable suggestions. We thank Janice A. Taylor and James R. Talaska of the Advanced Microscopy Core Facility at the University of Nebraska Medical Center for providing assistance with confocal microscopy. We also thank Dr. Andres Merits for kindly providing the nsP4 antibody. This study was supported by NIH/NIAID 1R21AI140026-01 (SPR & BD) and start-up funds (SPR).

bioRxiv preprint doi: https://doi.org/10.1101/780791; this version posted September 24, 2019. The copyright holder for this preprint (which was not certified by peer review) is the author/funder, who has granted bioRxiv a license to display the preprint in perpetuity. It is made available under aCC-BY-NC-ND 4.0 International license.

References

1. Higashi N MA, Tabata K, Nagatomo Y. Electron microscope study of development of Chikungunya virus in green monkey kidney stable (VERO) cells. Virology. 1967;33(1):55-69.
2. Morrison CR, Plante KS, Heise MT. Chikungunya Virus: Current Perspectives on a Reemerging Virus. Microbiol Spectr. 2016;4(3).
3. Zeller H, Van Bortel W, Sudre B. Chikungunya: Its History in Africa and Asia and Its Spread to New Regions in 2013-2014. J Infect Dis. 2016;214(suppl 5):S436-S40.
4. Yactayo S, Staples JE, Millot V, Cibrelus L, Ramon-Pardo P. Epidemiology of Chikungunya in the Americas. J Infect Dis. 2016;214(suppl 5):S441-S5.
5. Powers AM, Logue CH. Changing patterns of chikungunya virus: re-emergence of a zoonotic arbovirus. J Gen Virol. 2007;88(Pt 9):2363-77.
6. Cunha RVD, Trinta KS. Chikungunya virus: clinical aspects and treatment - A Review. Mem Inst Oswaldo Cruz. 2017;112(8):523-31.
7. Chang AY, Encinales L, Porras A, Pacheco N, Reid SP, Martins KAO, et al. Frequency of Chronic Joint Pain Following Chikungunya Virus Infection: A Colombian Cohort Study. Arthritis Rheumatol. 2018;70(4):578-84.
8. Amaral JK, Taylor PC, Teixeira MM, Morrison TET, Schoen RT. The Clinical Features, Pathogenesis and Methotrexate Therapy of Chronic Chikungunya Arthritis. Viruses. 2019;11(3).
9. Sales G, Barbosa ICP, Canejo Neta LMS, Melo PL, Leitao RA, Melo HMA. Treatment of chikungunya chronic arthritis: A systematic review. Rev Assoc Med Bras (1992). 2018;64(1):63-70.
10. K. Krishnamoorthy KTH, A. Krishna Kumari & L.K. Das. Burden of chikungunya in India: estimates of disability adjusted life years (DALY) lost in 2006 epidemic
J Vector Borne Dis. 2009;46(1):26–35.
11. Goupil BA, McNulty MA, Martin MJ, McCracken MK, Christofferson RC, Mores CN. Novel Lesions of Bones and Joints Associated with Chikungunya Virus Infection in Two Mouse Models of Disease: New Insights into Disease Pathogenesis. PLoS One. 2016;11(5):e0155243.
12. Gardner J, Anraku I, Le TT, Larcher T, Major L, Roques P, et al. Chikungunya virus arthritis in adult wild-type mice. J Virol. 2010;84(16):8021-32.
13. Chen W, Foo SS, Rulli NE, Taylor A, Sheng KC, Herrero LJ, et al. Arthritogenic alphaviral infection perturbs osteoblast function and triggers pathologic bone loss. Proc Natl Acad Sci U S A. 2014;111(16):6040-5.
14. Manimunda SP, Vijayachari P, Uppoor R, Sugunan AP, Singh SS, Rai SK, et al. Clinical progression of chikungunya fever during acute and chronic arthritic stages and the changes in joint morphology as revealed by imaging. Trans R Soc Trop Med Hyg. 2010;104(6):392-9.
15. Malvy D, Ezzedine K, Mamani-Matsuda M, Autran B, Tolou H, Receveur MC, et al. Destructive arthritis in a patient with chikungunya virus infection with persistent specific IgM antibodies. BMC Infect Dis. 2009;9:200.
16. Wei X, Yang X, Han ZP, Qu FF, Shao L, Shi YF. Mesenchymal stem cells: a new trend for cell therapy. Acta Pharmacol Sin. 2013;34(6):747-54.

bioRxiv preprint doi: https://doi.org/10.1101/780791; this version posted September 24, 2019. The copyright holder for this preprint (which was not certified by peer review) is the author/funder, who has granted bioRxiv a license to display the preprint in perpetuity. It is made available under aCC-BY-NC-ND 4.0 International license.

17. Li M, Ikehara S. Bone-marrow-derived mesenchymal stem cells for organ repair. Stem Cells Int. 2013;2013:132642.
18. Wang C, Meng H, Wang X, Zhao C, Peng J, Wang Y. Differentiation of Bone Marrow Mesenchymal Stem Cells in Osteoblasts and Adipocytes and its Role in Treatment of Osteoporosis. Med Sci Monit. 2016;22:226-33.
19. Wagner ER, Luther G, Zhu G, Luo Q, Shi Q, Kim SH, et al. Defective osteogenic differentiation in the development of osteosarcoma. Sarcoma. 2011;2011:325238.
20. Valenti MT, Dalle Carbonare L, Mottes M. Osteogenic Differentiation in Healthy and Pathological Conditions. Int J Mol Sci. 2016;18(1).
21. Mumtaz N, Koedam M, van den Doel PB, van Leeuwen J, Koopmans MPG, van der Eerden BCJ, et al. Zika virus infection perturbs osteoblast function. Sci Rep. 2018;8(1):16975.
22. Smirnov SV, Harbacheuski R, Lewis-Antes A, Zhu H, Rameshwar P, Kotenko SV. Bone-marrow-derived mesenchymal stem cells as a target for cytomegalovirus infection: implications for hematopoiesis, self-renewal and differentiation potential. Virology. 2007;360(1):6-16.
23. Hanna H, Mir LM, Andre FM. In vitro osteoblastic differentiation of mesenchymal stem cells generates cell layers with distinct properties. Stem Cell Res Ther. 2018;9(1):203.
24. Goupil BA, Mores CN. A Review of Chikungunya Virus-induced Arthralgia: Clinical Manifestations, Therapeutics, and Pathogenesis. Open Rheumatol J. 2016;10:129-40.
25. Cao J, Wei Y, Lian J, Yang L, Zhang X, Xie J, et al. Notch signaling pathway promotes osteogenic differentiation of mesenchymal stem cells by enhancing BMP9/Smad signaling. Int J Mol Med. 2017;40(2):378-88.
26. Meisel R, Heseler K, Nau J, Schmidt SK, Leineweber M, Pudelko S, et al. Cytomegalovirus infection impairs immunosuppressive and antimicrobial effector functions of human multipotent mesenchymal stromal cells. Mediators Inflamm. 2014;2014:898630.
27. Chalaem P, Chusri S, Fernandez S, Chotigeat W, Anguita J, Pal U, et al. Characterization of a Chikungunya virus strain isolated from banked patients' sera. Virol J. 2016;13(1):150.
28. Wischmann J, Lenze F, Thiel A, Bookbinder S, Querido W, Schmidt O, et al. Matrix mineralization controls gene expression in osteoblastic cells. Exp Cell Res. 2018;372(1):25-34.
29. Assis-Ribas T, Forni MF, Winnischofer SMB, Sogayar MC, Trombetta-Lima M. Extracellular matrix dynamics during mesenchymal stem cells differentiation. Dev Biol. 2018;437(2):63-74.
30. Wang W, Li P, Li W, Jiang J, Cui Y, Li S, et al. Osteopontin activates mesenchymal stem cells to repair skin wound. PLoS One. 2017;12(9):e0185346.
31. Tsai MT, Lin DJ, Huang S, Lin HT, Chang WH. Osteogenic differentiation is synergistically influenced by osteoinductive treatment and direct cell-cell contact between murine osteoblasts and mesenchymal stem cells. Int Orthop. 2012;36(1):199-205.
32. LOUIS C. GERSTENFELD JC, COLLEEN M. SHEA, KUBER SAMPATH, GEORGE L. BARNES, and THOMAS A. EINHORN. Chondrocytes Provide Morphogenic Signals That Selectively Induce Osteogenic Differentiation of Mesenchymal Stem Cells. JOURNAL OF BONE AND MINERAL RESEARCH. 2002;17(2):221-30.
33. F. VILLARS BG, T. AME´ DE´ E, S. DUTOYA, L. BORDENAVE, R. BAREILLE, AND J. AME´ DE´ E. Effect of HUVEC on human osteoprogenitor cell differentiation needs heterotypic gap junction communication. Am J Physiol Cell Physiol. 2001;282(4):775-85.

bioRxiv preprint doi: https://doi.org/10.1101/780791; this version posted September 24, 2019. The copyright holder for this preprint (which was not certified by peer review) is the author/funder, who has granted bioRxiv a license to display the preprint in perpetuity. It is made available under aCC-BY-NC-ND 4.0 International license.

34. Jeon OH, Panicker LM, Lu Q, Chae JJ, Feldman RA, Elisseeff JH. Human iPSC-derived osteoblasts and osteoclasts together promote bone regeneration in 3D biomaterials. Sci Rep. 2016;6:26761.
35. Chen Y-J, Shie M-Y, Hung C, Jr., Liu S-L, Huang T-H, Kao C-T. Osteoblasts subjected to tensile force induce osteoclastic differentiation of murine macrophages in a coculture system. Journal of Dental Sciences. 2015;10(1):81-7.
36. James Jam Jolly K-YC, Mohd Fozi Nur Farhana, Ekram Alias, Kien Hui Chua, Wan Nuraini Wan Hasan, Soelaiman Ima-Nirwana,. Optimization of the Static Human Osteoblast/Osteoclast Co-culture System. 2018;43(2):208-13.
37. Boyce BF, Xing L. Functions of RANKL/RANK/OPG in bone modeling and remodeling. Arch Biochem Biophys. 2008;473(2):139-46.
38. Geusens PP, Landewe RB, Garnero P, Chen D, Dunstan CR, Lems WF, et al. The ratio of circulating osteoprotegerin to RANKL in early rheumatoid arthritis predicts later joint destruction. Arthritis Rheum. 2006;54(6):1772-7.
39. Geusens P. The role of RANK ligand/osteoprotegerin in rheumatoid arthritis. Ther Adv Musculoskelet Dis. 2012;4(4):225-33.
40. Remuzgo-Martinez S, Genre F, Lopez-Mejias R, Ubilla B, Mijares V, Pina T, et al. Expression of osteoprotegerin and its ligands, RANKL and TRAIL, in rheumatoid arthritis. Sci Rep. 2016;6:29713.
41. Noret. 2012.
42. Li YG, Siripanyaphinyo U, Tumkosit U, Noranate N, A An, Tao R, et al. Chikungunya virus induces a more moderate cytopathic effect in mosquito cells than in mammalian cells. Intervirology. 2013;56(1):6-12.
43. Kuss MA, Wu S, Wang Y, Untrauer JB, Li W, Lim JY, et al. Prevascularization of 3D printed bone scaffolds by bioactive hydrogels and cell co-culture. Journal of Biomedical Materials Research Part B: Applied Biomaterials. 2018;106(5):1788-98.
44. Birmingham E, Niebur GL, McHugh PE, Shaw G, Barry FP, McNamara LM. Osteogenic differentiation of mesenchymal stem cells is regulated by osteocyte and osteoblast cells in a simplified bone niche. European Cells and Materials. 2012;23:13-27.

Figure Legends

Fig 1. Experimental outline.

Fig 2. CHIKV infects and replicates in BMMSCs. BMMSCs were mock-infected or infected with CHIKV under acute viral infection: MOIs of 0.001, 0.01, 0.1 or 1.0 (A) Representative immunofluorescence images of cells fixed and immunostained at 24 hpi with antibodies against the viral nsP4 protein (red), Vimentin (green), and Hoechst

bioRxiv preprint doi: https://doi.org/10.1101/780791; this version posted September 24, 2019. The copyright holder for this preprint (which was not certified by peer review) is the author/funder, who has granted bioRxiv a license to display the preprint in perpetuity. It is made available under aCC-BY-NC-ND 4.0 International license.

nuclear stain (blue). Scale bar=20µm. (B) Viral nsP1 gene expression was quantified by qRT-PCR at 24 hpi. Bar graph shows fold change in gene expression. Fold change was calculated by 2^-ΔΔCt method. Error bars show ±SEM.

Fig 3. Osteogenic differentiation of BMMSCs and susceptibility of osteogenic cells to CHIKV infection. (A) Representative brightfield images of mock infected, differentiated and undifferentiated BMMSCs, stained with Alizarin Red at 7 and 14 dpd. Scale bar=0.2µm. (B) Viral nsP1 gene expression was quantified by qRT-PCR at 7 dpi. Bar graph shows fold change in gene expression in infected cells compared to mock-infected control. Fold change was calculated by 2^-ΔΔCt method. n=3. (C) Plaque assays were performed using culture supernatant of infected BMMSCs. n=3. Error bars show ±SEM. (D) Representative bright field images of morphological analysis of BMMSCs at 7 dpi to detect CPE. n=3. Scale bar=0.2 µm.

Fig 4. Effect of CHIKV infection on osteogenic cells. BMMSCs were mock-infected or infected with CHIKV under chronic viral infection at MOIs of 0.001 or 0.01. (A and B) Bar graphs show intracellular ALP activity detected by ALP activity assay at 7 and 14 dpi. ALP levels were normalized against total protein. n=5. Error bars show ±SEM. Significant changes are represented as p-values (**p<0.001) (C) Representative bright field images of infected and mock infected BMMSCs stained by ALP staining assay to detect extracellular ALP activity at 7 and 14 dpi. (D) Representative brightfield images of infected and mock infected BMMSCs, stained with Alizarin Red at 7 and 14 dpi. Scale bar=0.2 µm.

bioRxiv preprint doi: https://doi.org/10.1101/780791; this version posted September 24, 2019. The copyright holder for this preprint (which was not certified by peer review) is the author/funder, who has granted bioRxiv a license to display the preprint in perpetuity. It is made available under aCC-BY-NC-ND 4.0 International license.

Fig. S1. CHIKV infection produces CPE in BMMSCs. BMMSCs were infected at MOIs of 0.001, 0.01, 0.1 or 1.0. (A) Representative brightfield images of morphological analysis of BMMSCs at 48 hpi. Scale bar=0.2 µm. (B) Quantification of CPE was performed at 48 hpi using Viral ToxGlo assay. n=3. Error bars show ±SEM.

Fig. S2. CHIKV produces CPE in osteogenic cells. BMMSCs were mock-infected or infected with CHIKV under chronic viral infection: MOIs of 0.001 or 0.01. (A) Quantification of CPE was performed at 7 dpi using Viral ToxGlo assay. n=3. Error bars show ±SEM.

(B) Representative brightfield images of morphological analysis of BMMSCs at 14 dpi. Scale bar=0.2 µm. (C) Quantification of CPE was performed at 14 dpi using Viral ToxGlo assay. n=3. Error bars show ±SEM.

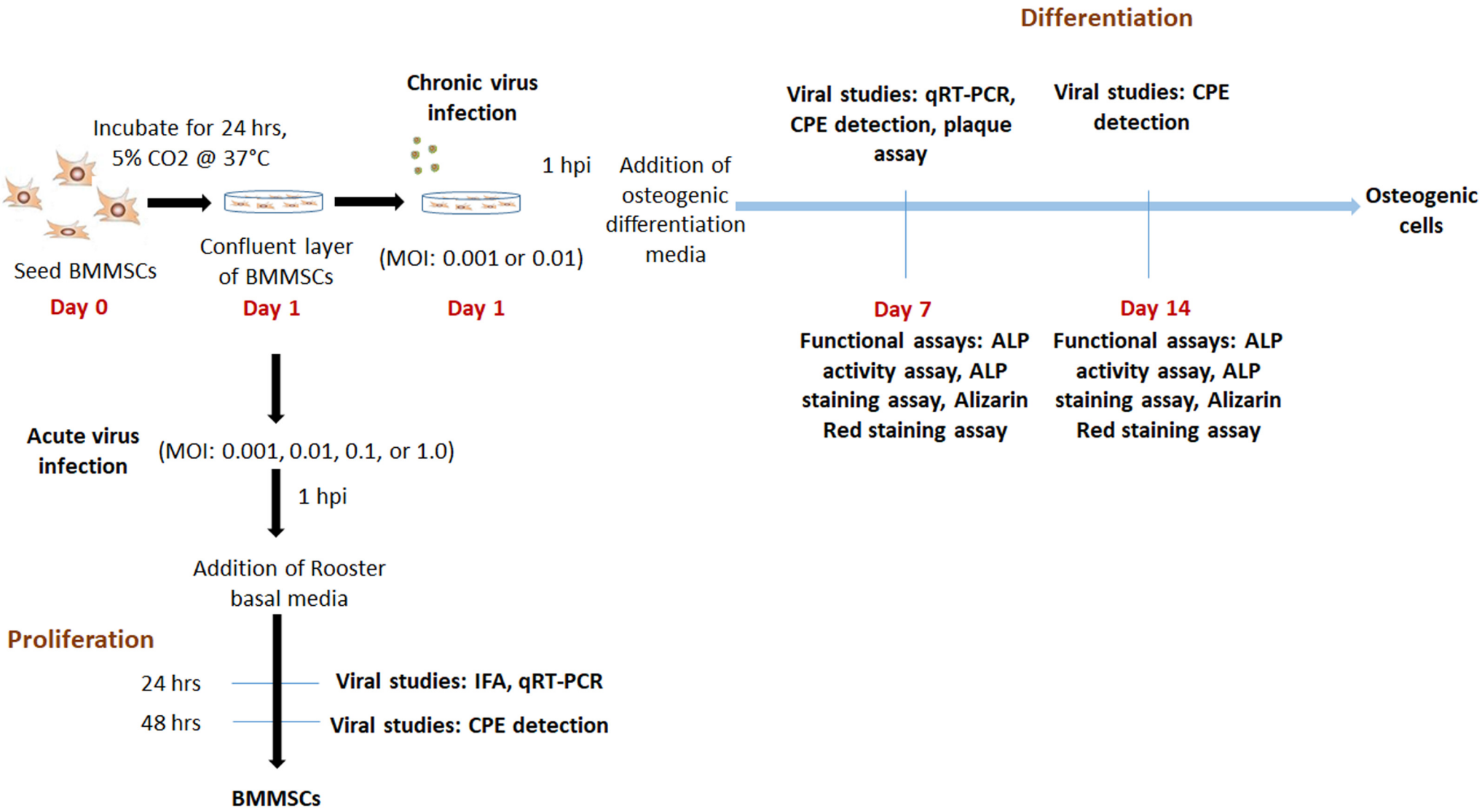
Differentiation
Chronic virus infection
Incubate for 24 hrs, 5% CO2 @ 37°C
1 hpi
Addition of osteogenic differentiation media
Viral studies: qRT-PCR, CPE detection, plaque assay
Viral studies: CPE detection
Osteogenic cells
Seed BMMSCs
Confluent layer of BMMSCs
(MOI: 0.001 or 0.01)
Day 0
Day 1
Day 1
Day 7
Day 14
Functional assays: ALP activity assay, ALP staining assay, Alizarin Red staining assay
Functional assays: ALP activity assay, ALP staining assay, Alizarin Red staining assay
Acute virus infection
(MOI: 0.001, 0.01, 0.1, or 1.0)
1 hpi
Addition of Rooster basal media
Proliferation
24 hrs
Viral studies: IFA, qRT-PCR
48 hrs
Viral studies: CPE detection
BMMSCs

bioRxiv preprint doi: https://doi.org/10.1101/780791; this version posted September 24, 2019. The copyright holder for this preprint (which was not certified by peer review) is the author/funder, who has granted bioRxiv a license to display the preprint in perpetuity. It is made available under aCC-BY-NC-ND 4.0 International license.

A)

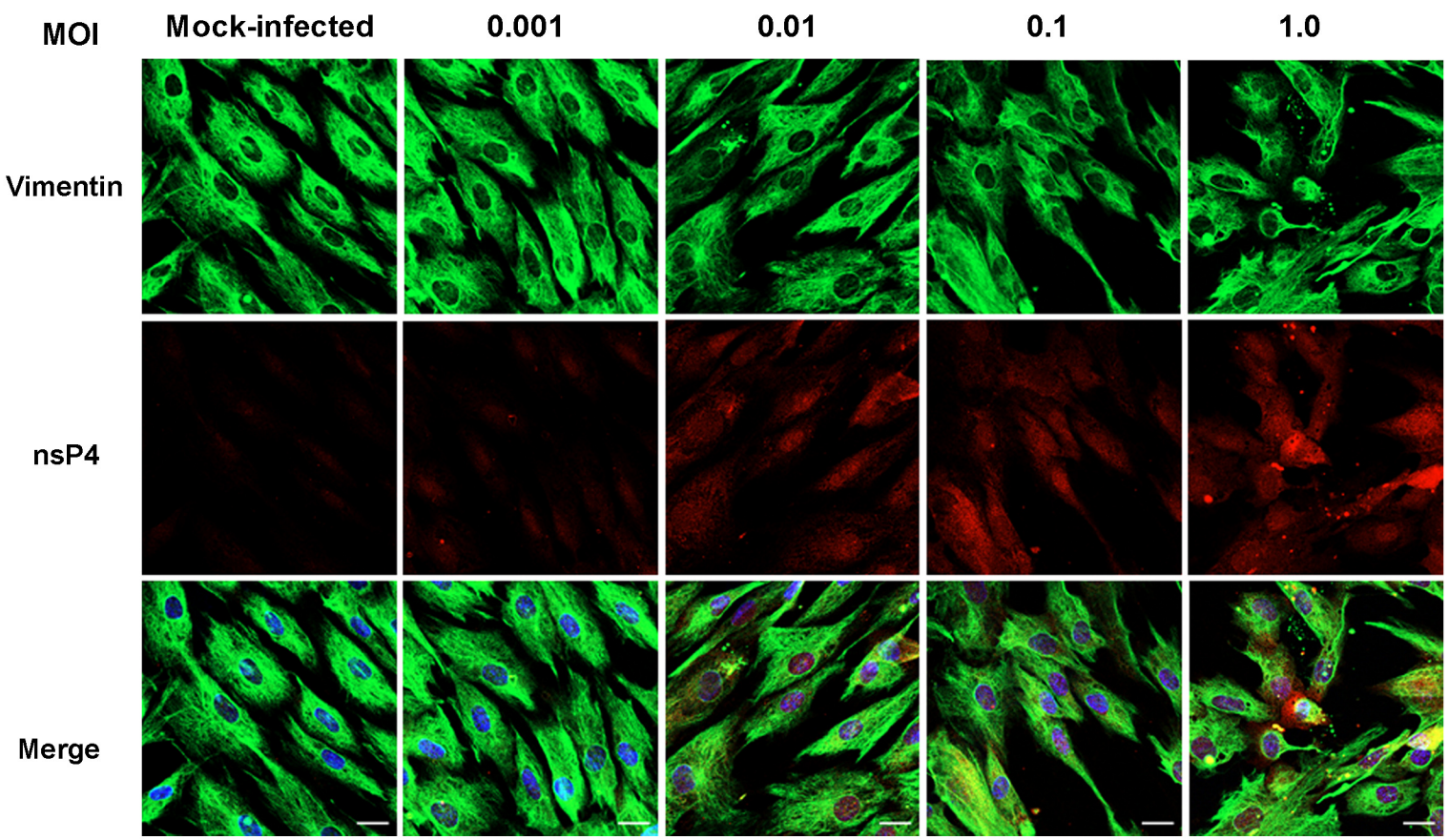

B)

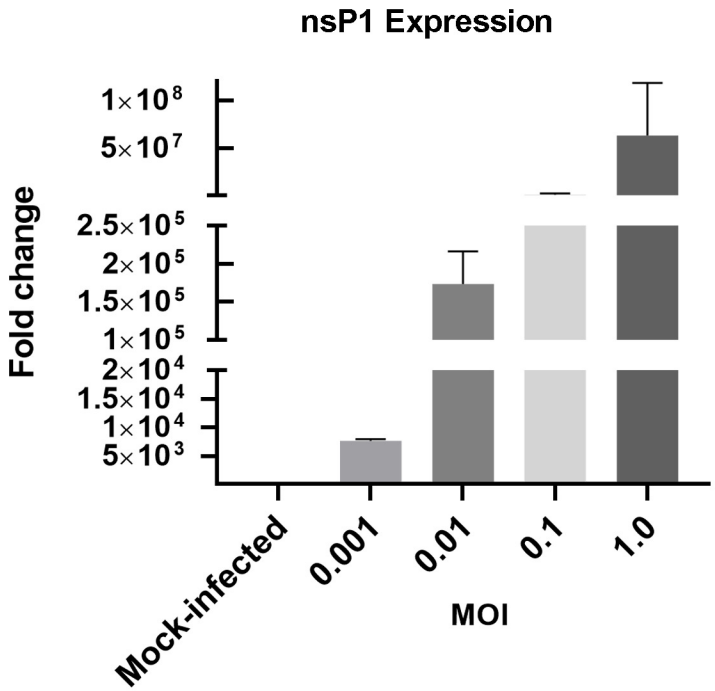

bioRxiv preprint doi: https://doi.org/10.1101/780791; this version posted September 24, 2019. The copyright holder for this preprint (which was not certified by peer review) is the author/funder, who has granted bioRxiv a license to display the preprint in perpetuity. It is made available under aCC-BY-NC-ND 4.0 International license.

A)

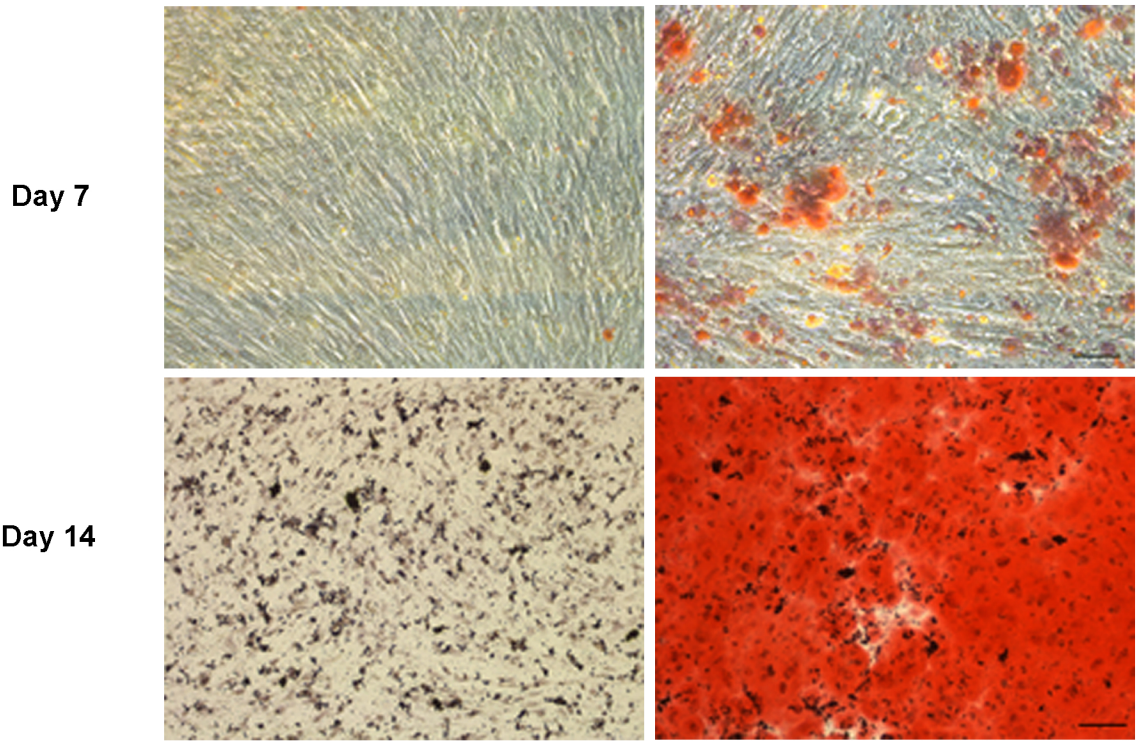

B)

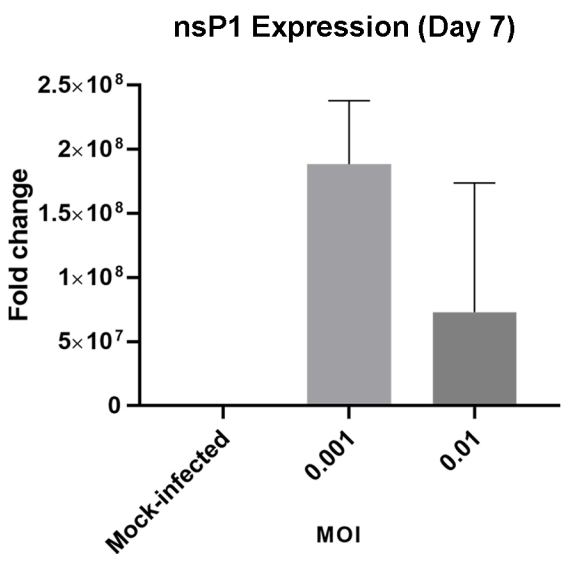

C)

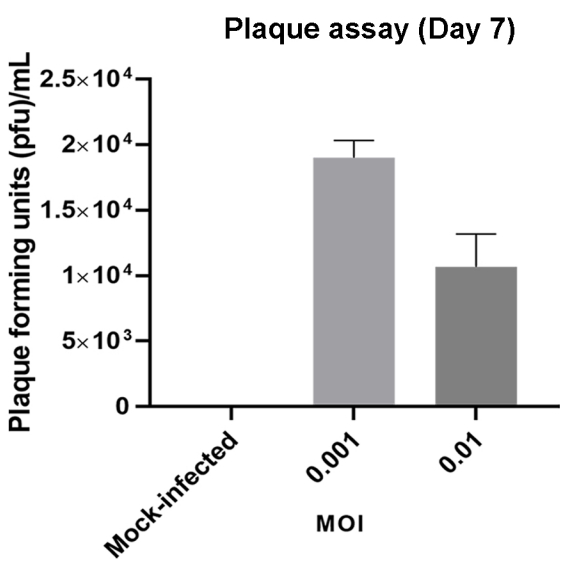

D)

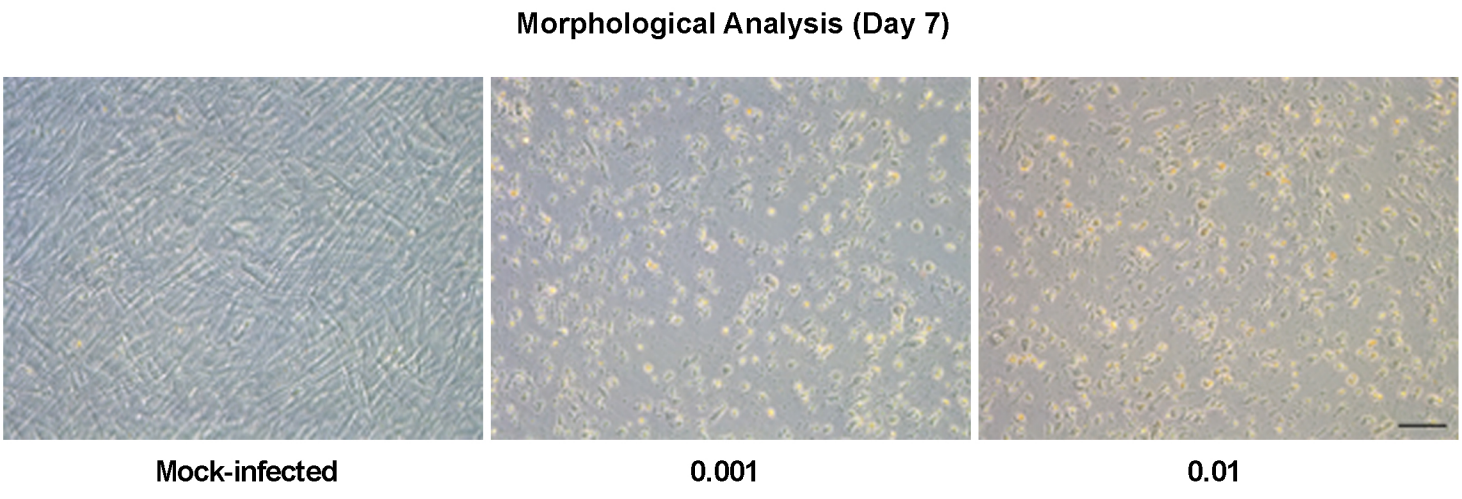

bioRxiv preprint doi: https://doi.org/10.1101/780791; this version posted September 24, 2019. The copyright holder for this preprint (which was not certified by peer review) is the author/funder, who has granted bioRxiv a license to display the preprint in perpetuity. It is made available under aCC-BY-NC-ND 4.0 International license.

A)

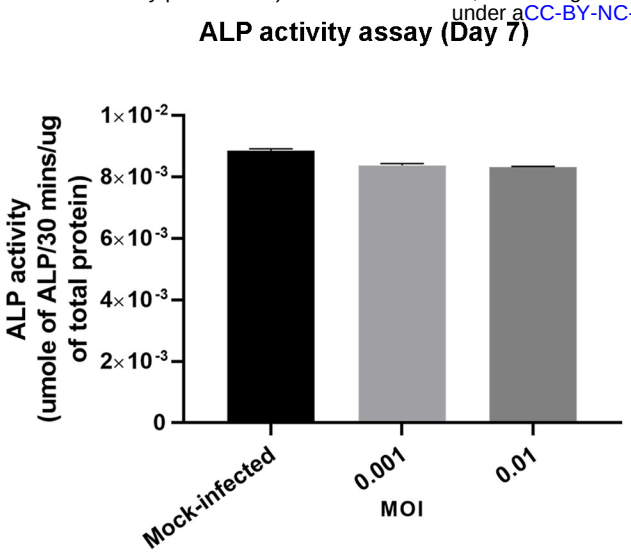

B)

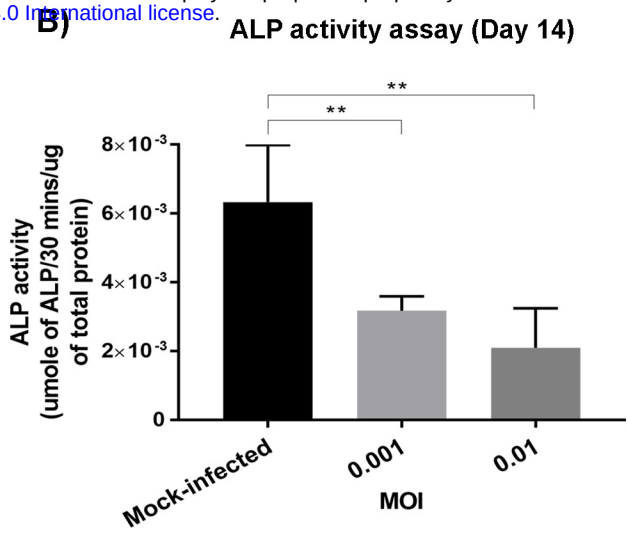

C)

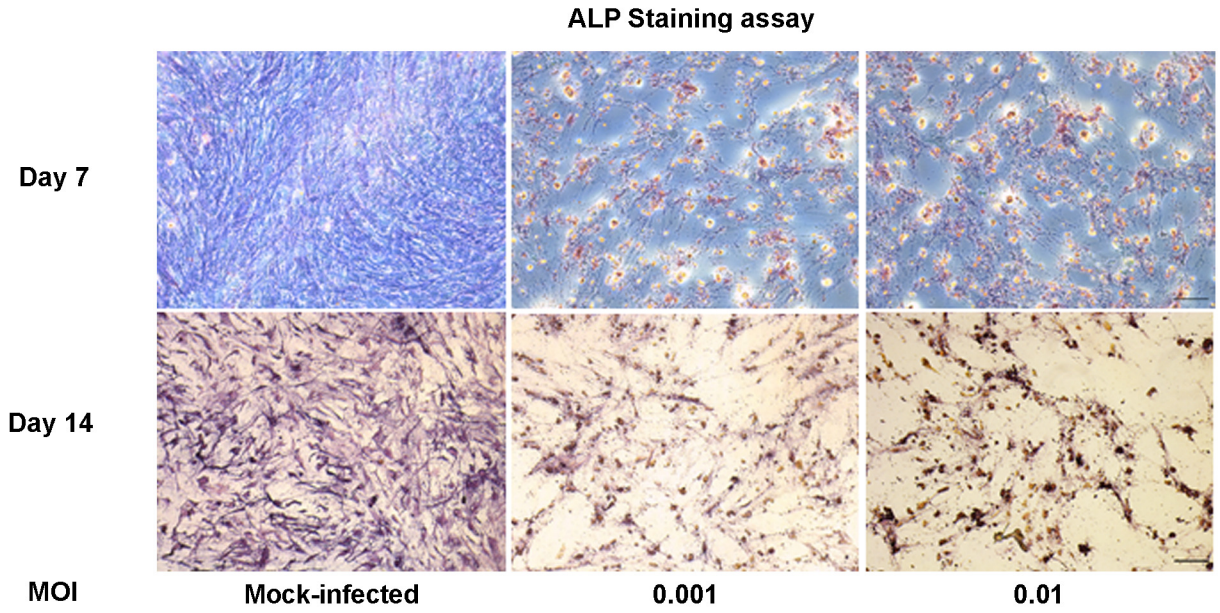

D)